Available online at www.sciencedirect.com
ScienceDirect
Journal of the European Ceramic Society 28 (2008) 2895–2901
www.elsevier.com/locate/jeurceramsoc

Mechanical properties and damage tolerance of Y_2SiO_5

Ziqi Sun [a,b], Jingyang Wang [a], Meishuan Li [a], Yanchun Zhou [a,*]

[a] *Shenyang National Laboratory for Materials Science, Institute of Metal Research, Chinese Academy of Sciences, 72 Wenhua Road, Shenyang 110016, China*
[b] *Graduate School of Chinese Academy of Sciences, Beijing 100039, China*

Received 19 January 2008; received in revised form 14 April 2008; accepted 25 April 2008
Available online 12 June 2008

Abstract

Y_2SiO_5 has potential applications as functional–structural ceramic and environmental/thermal barrier coating material. As an important grain-boundary phase in the sintered Si_3N_4, it also influences the mechanical and dielectric performances of the host material. In this paper, we present the mechanical properties of Y_2SiO_5 including elastic moduli, hardness, strength and fracture toughness, and try to understand the mechanical features from the viewpoint of crystal structure. Y_2SiO_5 has low shear modulus, low hardness, as well as high capacity for dispersing mechanical damage energy and for resisting crack penetration. Particularly, it can be machined by cemented carbides tools. The crystal structure characteristics of Y_2SiO_5 suggest the low-energy weakly bonded atomic planes crossed only by the easily breaking Y–O bonds as well as the rotatable rigid SiO_4 tetrahedra are the origins of low shear deformation, good damage tolerance and good machinability of this material. TEM observations also demonstrate that the mechanical damage energy was dispersed in the form of the micro-cleavages, stacking faults and twins along these weakly bonded atomic planes, which allows the "microscale-plasticity" for Y_2SiO_5.

Keywords: Y_2SiO_5; Mechanical properties; Damage; Strength; Fracture

1. Introduction

Yttrium silicate (Y_2SiO_5) is an important laser crystal that has been synthesized by chemical method since 1963.[1] Most research activities are related to rare earth (Ce^{3+}, Eu^{3+}, etc.)-doped Y_2SiO_5 crystals used as blue phosphor or Cr^{4+}-doped Y_2SiO_5 as saturable-absorber Q-switch laser.[2–4] As an important phase in the SiO_2–Y_2O_3–Si_3N_4 phase diagram, Y_2SiO_5 is frequently identified as a precipitated phase at the grain-boundaries of sintered Si_3N_4 with Y_2O_3 or $Y_2O_3 + SiO_2$ as sintering aid.[5–7] And it has been proven that Y_2SiO_5 has the capability of improving the high-temperature performance of silicon nitride.[8–10] The melting point of Y_2SiO_5 is 1950 °C, which also guaranties its potential high-temperature structural applications.[11] Recently, some investigations have demonstrated that Y_2SiO_5 is a promising high-temperature functional–structural material. Ching et al.[12] calculated the dielectric properties of Y–Si–O ceramics, the dielectric constant for Y_2SiO_5 is as low as 3.4, indicating its potential applications as microwave devices and high-temperature dielectric components. Y_2SiO_5 has also attracted the attention of material scientists due to its good chemical stability and desired match of thermal expansion coefficient ($8.36 \times 10^{-6}\,K^{-1}$ for polycrystalline sample[13]) with some non-oxide materials such as silicon-based ceramics, C/C composites and so on, especially combined with $Y_2Si_2O_7$.[14–17] Moreover, Y_2SiO_5 has a low evaporation rate as well as low oxygen permeability constant (10^{-10} kg/(m s)) at temperatures even up to 1700 °C, which endows Y_2SiO_5 as excellent oxidation-resistant coatings.[18] Practically, Y_2SiO_5 coatings on SiC-based ceramics can improve the high-temperature oxidation resistance of the substrate efficiently.[19,20] As a promising material for structural and coating applications, the fundamental mechanical and thermal properties of bulk Y_2SiO_5 are still in dearth due to the difficulty in preparing single-phase Y_2SiO_5. During the synthesis of Y_2SiO_5, undesired phases, such as $Y_{4.67}(SiO_4)_3O$, $Y_2Si_2O_7$, etc., and the incomplete transformed polymorphs like low-temperature phase (X1–Y_2SiO_5), always appear as impurities.

* Corresponding author at: High-performance Ceramic Division, Shenyang National Laboratory for Materials Science, Institute of Metal Research, Chinese Academy of Sciences, 72 Wenhua Road, Shenyang 110016, China.
Tel.: +86 24 23971765; fax: +86 24 23891320.
E-mail address: yczhou@imr.ac.cn (Y. Zhou).

0955-2219/$ – see front matter © 2008 Elsevier Ltd. All rights reserved.
doi:10.1016/j.jeurceramsoc.2008.04.029

Very recently, we successfully synthesized single-phase X2–Y_2SiO_5 powders (here after written as Y_2SiO_5 for brevity) from Y_2O_3 and SiO_2 powders utilizing a simple solid–liquid reaction method.[21] In this paper, the mechanical properties of single-phase bulk Y_2SiO_5 ceramic including elastic moduli, hardness, strength and fracture toughness were measured. Since the performances of a material are intimately correlated with its structure, here the relationship between the crystal structure and mechanical properties of Y_2SiO_5 was investigated in detail. To support our speculations on deformation mechanism, transmission electron microscope (TEM) observations on the deformed samples were carried out. These fundamental mechanical properties of Y_2SiO_5 are beneficial for further engineering application of this novel ceramic as well as for better understanding the performance of Y_2O_3-doped Si_3N_4.

2. Experimental procedure

2.1. Crystal structure and materials preparation

The equilibrium crystal structure of Y_2SiO_5 was calculated in the framework of density functional theory by using CASTEP code.[22] The Vanderbilt-type ultrasoft pseudopotential and generalized gradient approximation were employed for the geometry optimization.

The Y_2SiO_5 powders were synthesized via a solid–liquid reaction method, wherein the initial yttria and silica powders were calcined with 3 mol% $LiYO_2$ additive at 1500 °C for 2 h in air. The bulk material with a final density of 98% was obtained by pressureless sintering the as-synthesized powders at 1500 °C for 60 min in air. Details of the preparation procedure can be found in our previous work.[21] Microstructure observation of the thermal etched specimens was performed in a SUPERA 35 scanning electron microscope (SEM, LEO, Oberkochen, Germany) equipped with an Oxford energy dispersive X-ray spectroscope.

To understand the damage mechanism, the Y_2SiO_5 ceramic was indented at room temperature with a 4.7-mm WC ball using 300 N load. Thin-foil specimens cut from regions containing indentations for TEM observations were prepared by slicing, mechanical grinding, dimpling, and finally ion milling. A 200 kV JEM-2010 TEM (JEOL, Tokyo, Japan) and a 300 kV Tecnai G^2 F30 TEM (FEI, Eindhoven, Netherlands) were used, respectively, for selected area electron diffraction analysis and high-resolution imaging.

2.2. Tests of mechanical properties

Young's modulus and shear modulus were tested on rectangular bars (3 mm × 11 mm × 39 mm) using the impulse-excited resonance method (resonance frequency and damping analyzer, IMCE, Diepenbeek, Belgium). The first resonance mode was chosen to determine the Young's modulus. The bulk modulus of Y_2SiO_5 was evaluated from the relationship between E (Young's modulus), G (shear modulus) and ν (Poisson's ratio), $B = (GE/3(3G - E))$

The Vickers microhardness was measured at loads of 0.5, 1, 3, 5, 10, 30 and 50 N with a dwell time of 15 s. To estimate the damage tolerance of the material, indentations on 3 mm × 4 mm × 36 mm flexural specimens were performed using a Vickers indenter under loads of 10, 30, 50, 100, and 200 N. One diagonal of the indenter was parallel to the length of the specimen. The residual strength after indentation was determined by four-point bending.

The flexural strength was determined via three-point bending test using samples with dimensions of 3 mm × 4 mm × 36 mm. In addition, the samples with a size of 2 mm × 2 mm × 4 mm were used for compression test and the height of them set parallel to the direction of compression. The crosshead speed in both flexural and compressive tests was 0.5 mm/min.

Fracture toughness was measured using Chevron-notched beam (CNB) method on the specimens with dimensions of 3 mm × 4 mm × 45 mm. Chevron notches were introduced by diamond-coated wheel slotting. The thickness of blade is 0.054 mm and the width of the notches is 0.14 mm. Four-point bending tests with a crosshead speed of 0.05 mm/min were performed for fracture toughness measurements.

Table 1
Y–O, Si–O and O–O bond lengths in Y_2SiO_5

Bond	Component	Bond length (Å)
Si–O	Si–O1[a]	1.639
	Si–O2[a]	1.631
	Si–O3[a]	1.608
	Si–O4[a]	1.626
Y–O	Y1–7O polyhedron	2.195[b]
		2.526[c]
	Y2–6O polyhedron	2.196[b]
		2.270[c]
O–O	Inner Si–4O tetrahedron	2.651[b]
		2.772[c]
	Outer Si–4O tetrahedron	2.538[b]
		2.944[c]

[a] Si–4O tetrahedron.
[b] minimum bond length.
[c] maximum bond length.

3. Results and discussion

3.1. Crystal structure

The equilibrium crystal structure of Y_2SiO_5 ($B2/b$, 15) was obtained using the Cambridge Sequential Total Energy Package (CASTEP) code[22] and the crystal structure parameters are in good agreement with those reported by Ching et al., who have investigated comprehensively into the electronic structures of compounds in Y–Si–O system.[12,23] As shown in Fig. 1(a), the unit cell of Y_2SiO_5 contains 32 atoms with two nonequivalent Y sites, denoted as Y1 and Y2, one Si site, and five O sites. Table 1 lists the corresponding atomic bond lengths in the equilibrium crystal structure. Y1 bonds to seven O atoms with bond lengths ranging from 2.195 to 2.526 Å, and Y2 bonds to six O atoms in the range over 2.196–2.270 Å. While Si is tetrahedrally surrounded by four O atoms with bond lengths ranging from 1.608 to 1.639 Å. O–O bonds are of antibonding

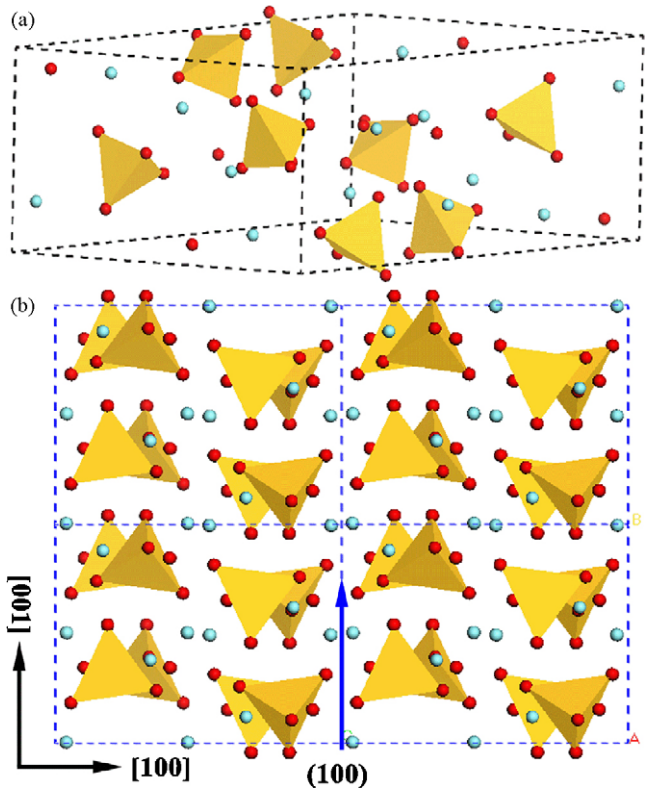

Fig. 1. Crystal structure of Y_2SiO_5, (a) unit cell and (b) projected $2 \times 2 \times 1$ supercell on the (0 1 0) crystal plane.

characteristics and repelling with each other. The bond lengths in Table 1 suggest a much stronger bonding character of Si–O bonds in SiO_4 tetrahedra than Y–O bonds in YO_6 or YO_7 polyhedra. Fig. 2 illustrates the projected density of states of Y_2SiO_5. The lowest lying states from −21 to −14 eV originate from "semi-core" valence electrons, which have little contribution to the chemical bonding. The Si–O covalent bonding states extend in a lower energy level from −6.5 to −3 eV with a localized Sis–Op and Sip–Op bonding characteristics, and Y–O bonding sates occupy the higher energy level from −3.3 eV to the Fermi level with a dominant but less localized Yd–Op bonding characteristics. From the viewpoint of bonding energy, the Si–O bonds locate in lower energy level and have a high bonding strength; and the Y–O bonds extend in higher energy level and exhibit weaker bonding strength. The whole crystal structure of Y_2SiO_5 is, therefore, characterized as rigid SiO_4 tetrahedrons "weakly linked" by YO_6 and YO_7 units. This structural feature is quite similar to that of $LaPO_4$ monazite ($P2_1/n$), which is characterized by continuous strongly bonded PO_4 tetrahedral glued by LaO_9 polyhedron with weak bonds.[22] $LaPO_4$ is well known as a weak interface material in fiber-reinforced ceramic-matrix composites,[24] and the weakly bonded atomic planes constituted of the long La–O bonds are reported to be the source of machinability and low shear deformation resistance of this material.[22] Fig. 1(b) is the projection of $2 \times 2 \times 1$ Y_2SiO_5 supercell on the (0 1 0) crystal plane. In close resemblance to the crystal structure of $LaPO_4$, weakly bonded (1 0 0) atomic planes crossed by long Y–O bonds in Y_2SiO_5 are noticed, as indicated by the arrow ((1 0 0) is the most obvious weakly bonded atomic planes but not the only one).

3.2. Mechanical properties

Fig. 3 shows a SEM micrograph of polished and then thermal etched surface of as-sintered Y_2SiO_5 that was pressureless sintered at 1500 °C for 60 min in air. The microstructure reveals equiaxial grains and the grain size is 6 μm on average. On the etched surface, owing to the rapid cooling rate after thermal etching, a few microcracks appear.

Fig. 4(a) shows the Vickers hardness of Y_2SiO_5 as a function of indentation load. It is noticed that the Vickers hardness depends on the applied load and asymptotically approaches a plateau value of about 5.3 GPa at high loads. SEM observation of the indent produced under 30 N load (insert in Fig. 4(a)) shows no apparent damage region except for some cracks around the indentation. Fig. 4(b) is a high magnification of the tortuous extension path from a main crack with a number of deflections and bridgings. These features imply that Y_2SiO_5 is capable of local energy dissipation and is hence resistant to crack propagation upon loading.

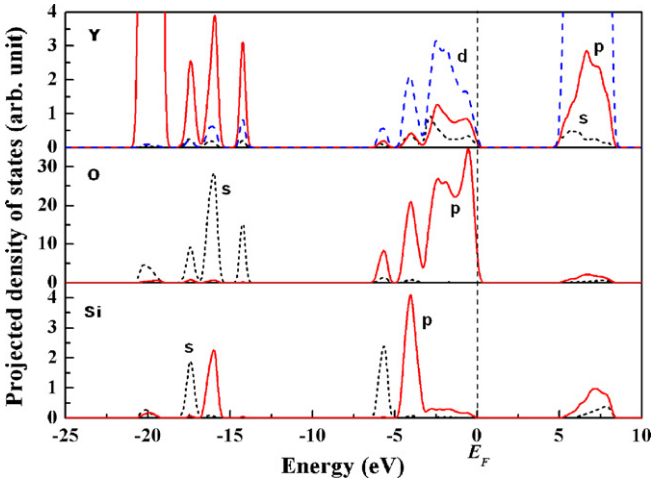

Fig. 2. Projected electronic density of states of Y_2SiO_5.

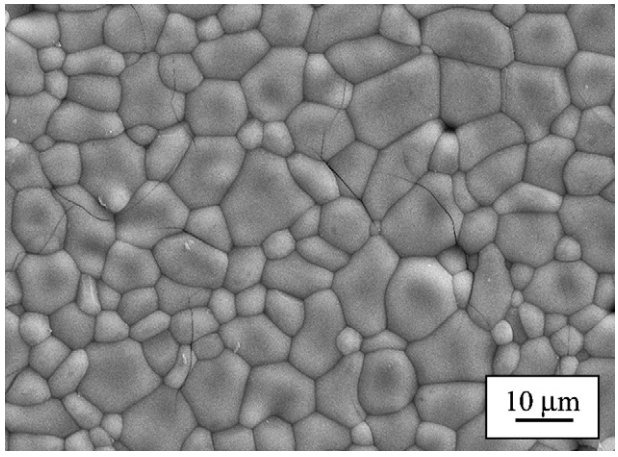

Fig. 3. Microstructure of sintered Y_2SiO_5.

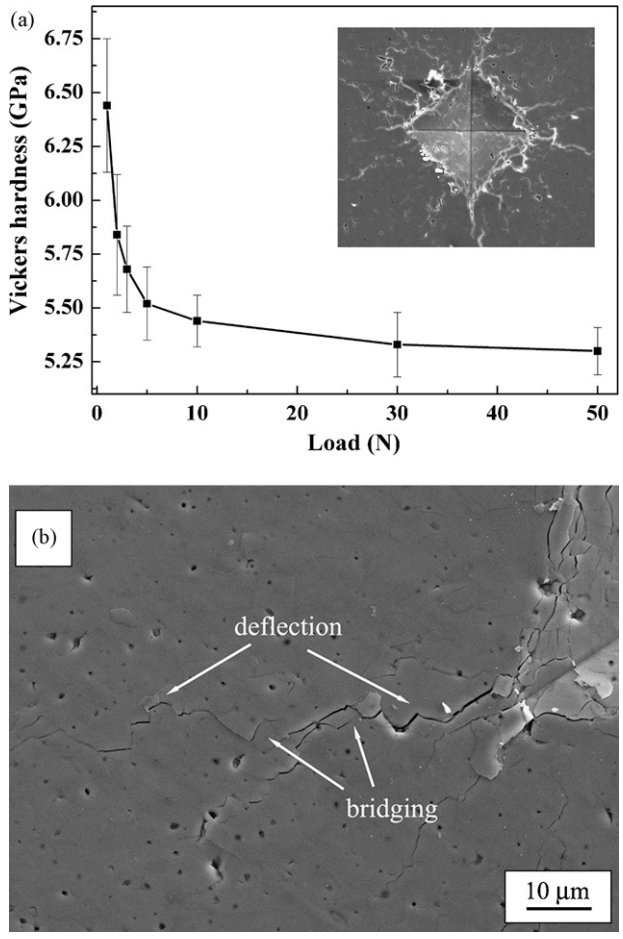

Fig. 4. (a) Vickers hardness vs. load, the inset figure is the 30 N indentation surface and (b) high magnification of crack deflection and bridging for a main crack produced at 30 N load.

The fracture surface of Y_2SiO_5 after three-point bending test, as shown in Fig. 5, exhibits a characteristic of both intergranular and intragranular fracture, as well as many sharp steps caused by crack deflection as cracks penetrating inside grains. The fracture energy was thus consumed by virtue of crack deflection.

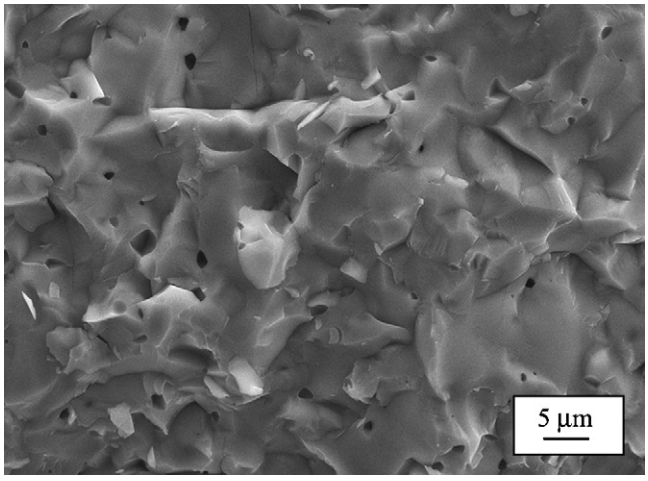

Fig. 5. The fracture surface of Y_2SiO_5 after bending.

All the measured mechanical properties of Y_2SiO_5 ceramic are summarized in Table 2, together with those of γ-$Y_2Si_2O_7$[25] and $LaPO_4$[26,27] for comparison. One can find that these ceramics have close values for some mechanical parameters: bending strength, Young's modulus and bulk modulus. However, Y_2SiO_5 exhibits lower hardness and shear modulus than γ-$Y_2Si_2O_7$ and $LaPO_4$, but higher fracture toughness than $LaPO_4$. Technically, γ-$Y_2Si_2O_7$ and $LaPO_4$ have been found to be machinable by conventional cemented carbides tools due to their low shear deformation resistance.[25–27] The resemblance of Y_2SiO_5 to γ-$Y_2Si_2O_7$ and $LaPO_4$ in the mechanical properties suggests that Y_2SiO_5 may also possess lower shear deformation resistance and machinability.

3.3. Damage tolerance and machinability

By analyzing the overall mechanical properties of Y_2SiO_5, it is speculated that this material is tolerant of damage. The Vickers indentation surface under 30 N load (the inset in Fig. 4(a)) takes on an appearance of few short cracks in the vicinity of indentation, wherein crack propagation is hindered by deflecting, bridging and branching (Fig. 4(b)). This kind of crack extension mode is helpful in dissipating the fracture energy and terminating the cracks in a local zone, which endows Y_2SiO_5 with good damage tolerance. The typical characteristics of decreased microhardness with increasing load, as well as the crack extension mode support the fact that Y_2SiO_5 has microscale-plasticity. This conjecture on microscale-plasticity is corroborated by the low H_v/E ratio. For most ceramics the H_v/E values are in the range of 0.02–0.1, whereas for most metals the ratios change between 0.001 and 0.03.[28] The H_v/E ratio for Y_2SiO_5 ceramic is only 0.042, implying that this ceramic might be of microplasticity.

To further prove the hypothesis that Y_2SiO_5 is a damage tolerance material, the four-point bending strength as a function of indentation loads was determined (Fig. 6). The asymptotic slope obtained at high indentation loads can be used as an indicator

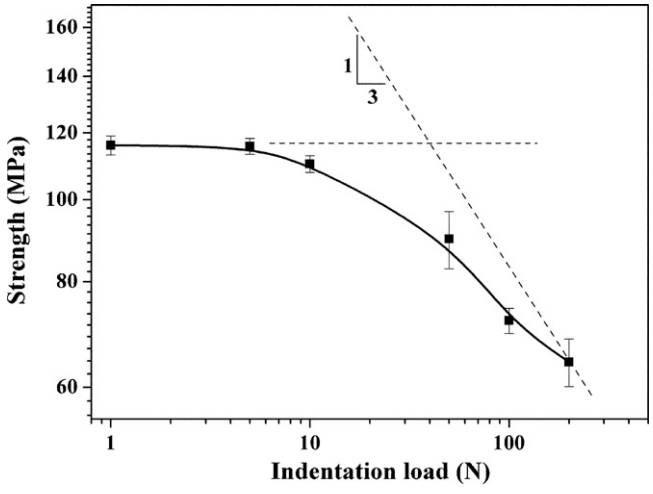

Fig. 6. Four-point flexural strength vs. indentation load. The inclined dashed line has a slope of −1/3, which is the expected behavior for a perfectly brittle ceramic.

Table 2
Summary of the mechanical properties of Y_2SiO_5, γ-$Y_2Si_2O_7$ and $LaPO_4$

	E (GPa)	G (GPa)	υ	B (GPa)	σ_b (MPa)	σ_c (MPa)	K_{Ic} (MPa m$^{1/2}$)	H (GPa)
Y_2SiO_5	124 ± 2	47	0.31	108	116 ± 3	620 ± 13	1.85 ± 0.17	5.3 ± 0.1
γ-$Y_2Si_2O_7$[a]	155 ± 3	61	0.27	112	135 ± 4	650 ± 20	2.12 ± 0.05	6.2 ± 0.1
$LaPO_4$[b]	134	53	0.28	99	102	/	1	4.9

[a] Ref.[25].
[b] Refs.[26,27].

of damage tolerance of materials—for perfectly brittle materials that slope corresponds to −1/3.[29] Here from Fig. 6, the slope for Y_2SiO_5 is less than −1/3, suggesting that it is a damage-tolerant ceramic.

Attributed to the combination of unique mechanical properties, such as low shear modulus, low hardness and high damage tolerance, Y_2SiO_5 can be drilled easily by a cemented carbide tool at a constant normal force of 50 N and at a speed of 600 rpm. The drilling rate was estimated to be roughly 0.7 mm/s. The drilled surface was found very complanate and partially covered with a layer of smeared debris. Assisted by a precision surface roughness meter (JB-4C roughness meter, Shanghai Taiming, Shanghai, China), the roughness (R_a) of the drilled surface was determined to be 5 μm. Based on these data, we can confidently conclude that Y_2SiO_5 is a machinable ceramic and its machinability is better than $Y_2Si_2O_7$. The very similar mechanical properties between $LaPO_4$ and Y_2SiO_5 also imply the promising application of Y_2SiO_5 as a novel weak interfacial phase for fiber-reinforced ceramic-matrix composites.

3.4. Origin of damage tolerance

It is well documented that the mechanical properties of a material are innately correlated to its crystal structure and chemical bonding. The origin of high damage tolerance and machinability for Y_2SiO_5 can be found by the investigation on its deformation mechanism. In the case of $LaPO_4$ monazite, whose structure is characterized by continuous strongly bonded PO_4 tetrahedral and LaO_9 polyhedron with weak bonds, the typical deformation mechanism is the weak La–O bonds accommodating the locally inhomogeneous shear strain and thus leading to the intrinsically low shear deformation resistance, while the rigid PO_4 tetrahedra remaining almost unchanged.[22] Analogously, the longer and weaker Y–O bonds in Y_2SiO_5 may respond to the applied mechanical perturbations more significantly than the strong Si–O bonds. When damage occurs, the bond breaking mainly takes place at Y–O bonds in Y_2SiO_5 along some specifically weak planes as indicated by the arrow in Fig. 1(b), while the rigid SiO_4 tetrahedra tends to release the energy by rotation. This suggests that these weakly bonded planes can act as low-energy interfaces favorable for cleavage, slip or twinning, and the low shear resistance and ductility of Y_2SiO_5 should be derived from these weakly bonded atomic planes.

To prove the mechanical response modes of these weakly bonded interfaces, TEM observations on the deformed zone were conducted. Fig. 7 shows the TEM images of the Y_2SiO_5 samples after spherical indentation at room temperature. Fig. 7(a) reveals that the grains in the deformation zone are commonly micro-cleaved into a number of well-orientated sub-grains, suggesting that the micro-cleavage should be the major mechanism of energy dispersion upon mechanical damage. HRTEM image (Fig. 7(b)) show that abundant stacking faults and twins existed in the sub-grains. The right upper high-resolution TEM pattern in Fig. 7(b) presents a (1 0 0) twin along [3 $\bar{1}$ $\bar{1}$] shear direction as indicated by the corresponding electron diffraction pattern at the lower right of the figure. Hay et al.[30] has studied the deformation twinning modes in $LaPO_4$, and found that (1 0 0) twins are by far the most common ones in the deformed grains, and in particular, the key factor that determines

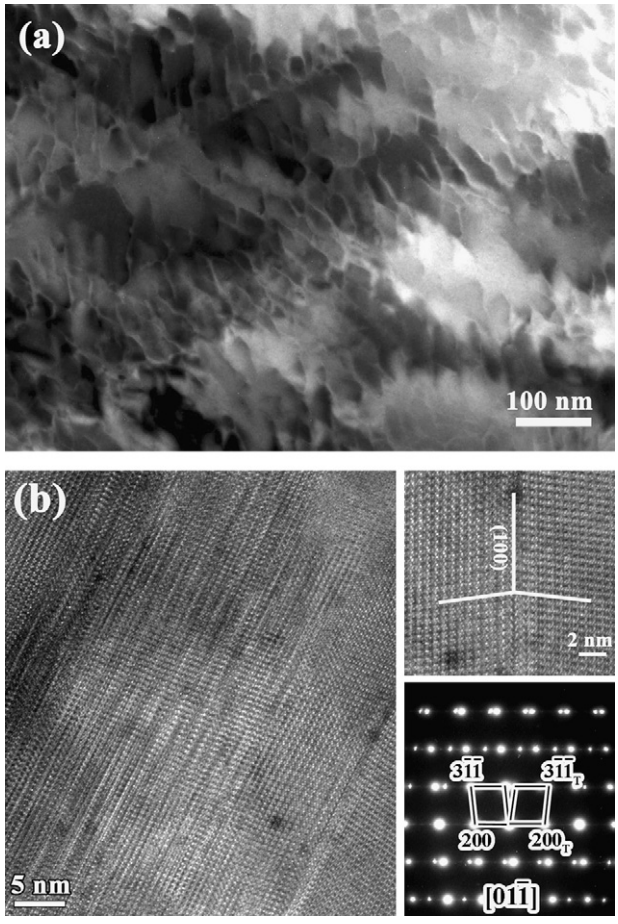

Fig. 7. TEM micrographs of indented Y_2SiO_5. (a) Bright image of the deformed Y_2SiO_5; (b) high-resolution TEM image of the sub-grain in (a) which is full of stacking faults and twining: the upper-right is an enlarged twining along (100) plane, and the lower-right is the corresponding SAED pattern for the upper twining.

the twining modes is the small atomic shuffles. Similar conclusions were carried out in $Er_2Si_2O_7$ and $Nb_2Si_2O_7$.[31,32] Based on a similar structure between $LaPO_4$ and Y_2SiO_5, the (1 0 0) low-energy weakly bonded atomic plane in Y_2SiO_5, as indicated in Fig. 1(b), is also expected to respond to the applied mechanical perturbations in the form of micro-cleavage, slip and twining. The common (1 0 0) twins may be aroused by the easily small atomic shuffles, or the rotations of SiO_4 tetrahedra.

The deformation mechanisms of Y_2SiO_5, therefore, can be summarized as follows: when subjected to mechanical damage, the strain energy can be accommodated in the form of micro-cleavage, slip and twining, and thus the material avoids the catastrophic failure. The ready response of Y_2SiO_5 to the mechanical disturbance is owing to the low-energy weakly bonded atomic planes crossed only by the comparatively weak Y–O bonds. The easily breaking Y–O bonds, small atomic shuffle or the rotatable rigid SiO_4 tetrahedra are the origins of low shear deformation, high damage tolerance and good machinability of Y_2SiO_5.

4. Conclusion

The mechanical properties of Y_2SiO_5 were comprehensively investigated in this paper. Based on the measured data, Y_2SiO_5 can be viewed as a potential machinable ceramic with low shear modulus, low hardness and high damage tolerance. The drilling test demonstrates that Y_2SiO_5 can be machined by cemented carbide tools. The DFT calculation reveals the weakly bonded atomic planes, which are crossed only by the easily breaking Y–O bonds, are the sources of low shear deformation resistance and good machinability of Y_2SiO_5. TEM observations also demonstrate a large number of micro-cleavages, stacking faults and twins along these weakly bonded atomic planes, which disperse the strain energy and thus allow "ductility" for Y_2SiO_5. The special mechanical features for Y_2SiO_5 imply its promising applications as components with complex shape and weak interfacial phase in fiber-reinforced ceramic-matrix composites.

Acknowledgements

This work was supported by the National Outstanding Young Scientist Foundation for Y.C. Zhou under Grant No. 59925208, Natural Sciences Foundation of China under Grant Nos. 50232040, 50302011, 90403027 and 50772114. The authors are also grateful to Dr. Z.J. Lin for his help on TEM observation.

References

1. Warshaw, J. and Roy, R., Crystal chemistry of rare earth sesquioxides, aluminates and silicates. *Prog. Sci. Technol., Rare Earths*, 1964, **1**, 203–221.
2. Shin, S. H., Jeon, D. Y. and Suh, K. S., Emission band shift of the cathodoluminescence of Y_2SiO_5:Ce phosphor affected by its concentration. *Jpn. J. Appl. Phys. Part 1*, 2001, **40**, 4715–4719.
3. Bottger, T., Sun, Y., Reinemer, G. J. and Core, R. L., Diode laser frequency stabilization to transient spectral holes and spectral diffusion in Er^{3+}:Y_2SiO_5 at 1536 nm. *J. Lumin.*, 2001, **94,95**, 565–568.
4. Deka, C., Chai, B., Shimony, Y., Zhang, X., Munin, E. and Bass, M., Laser performance of Cr^{4+}–Y_2SiO_5. *Appl. Phys. Lett.*, 1992, **61**, 2141–2143.
5. Liddell, K. and Thompson, D. P., X-ray-diffraction data for yttrium silicates. *Br. Ceram. Trans. J.*, 1986, **85**, 17–22.
6. Lange, F. F., Singhal, S. C. and Kuznicki, R. C., Phase relations and stability studies in the Si_3N_4–SiO_2–Y_2O_3 pseudoternary system. *J. Am. Ceram. Soc.*, 1977, **60**, 249–252.
7. Gauckler, L. J., Hohnke, H. and Tien, T. Y., The system Si_3N_4–SiO_2–Y_2O_3. *J. Am. Ceram. Soc.*, 1980, **63**, 35–37.
8. Cinibulk, M. K. and Thomas, G., Grain-boundary-phase crystallization and strength of silicon nitride sintered with a YSiAlON glass. *J. Am. Ceram. Soc.*, 1990, **73**, 1606–1612.
9. Lichvár, P., Šajgalík, P., Liška, M. and Galusek, D., CaO–SiO_2–Al_2O_3–Y_2O_3 glass as model grain boundary phases for Si_3N_4 ceramics. *J. Eur. Ceram. Soc.*, 2007, **27**, 429–436.
10. Chen, J., Ouyang, L., Rulis, P., Misra, A. and Ching, W. Y., Complex nonlinear deformation of nanometer intergranular glassy films in β-Si_3N_4. *Phys. Rev. Lett.*, 2005, **95** (No. 256103).
11. Levin, E. M., Robbins, C. R. and McMurdie, H. F., *Phase Diagrams for Ceramists-1969 Supplement*. The American Ceramic Society Inc., Columbus, OH, 1969, Fig. 2388, p. 76.
12. Ching, W. Y., Ouyang, L. and Xu, Y., Electronic and optical properties of Y_2SiO_5 and $Y_2Si_2O_7$ with comparisons to α-SiO_2 and Y_2O_3. *Phys. Rev. B*, 2003, **67** (No. 245108).
13. Sun, Z. Q., Zhou, Y. C. and Li, M. S., Thermal properties of single-phase Y_2SiO_5, Unpublished work.
14. Ogura, Y., Kondo, M. and Morimoto, T., Y_2SiO_5 as oxidation resistance coating for C/C composites. In *Proceedings of the 10th International Conference on Computational Material (ICCM-10), vol. IV*. Whistler, BC, Canada, 1995. p. 767.
15. Apricio, M. and Duran, A., Yttrium silicate coatings for oxidation protection of carbon–silicon carbide composites. *J. Am. Ceram. Soc.*, 2000, **83**, 1351–1355.
16. Wagner, S., Seifert, H. J. and Aldinger, F., High-temperature reaction of C/C–SiC composites with ceramic coatings. In *Proceedings of the 10th International Conference on Advances in Materials and Material Processing (ICAMMP-2002)*. Tata McGraw-Hill, New Delhi, 2002. p. 71.
17. Webster, J. D., Westwood, M. E., Hayes, F. H., Day, R. J., Taylor, R., Duran, A., Aparicio, M., Rebstock, K. and Vogel, W. D., Oxidation protection coatings for C/SiC based on yttrium silicate. *J. Eur. Ceram. Soc.*, 1998, **18**, 2345–2350.
18. Ogura, Y., Kondo, M., Morimoto, T., Notomi, A. and Sekigawa, T., Oxygen permeability of Y_2SiO_5. *Mater. Trans.*, 2001, **42**, 1124–1130.
19. Nowok, J. W., Kay, J. P. and Kulas, R. J., Thermal expansion and high-temperature phase transformation of the yttrium silicate Y_2SiO_5. *J. Mater. Res.*, 2001, **16**, 2251–2255.
20. Seifert, H. J., Wagner, S., Fabrichnaya, O., Lukas, H., Aldinger, F., Ullmann, T., Schmucker, M. and Schneider, H., Yttrium silicate coatings on chemical vapor deposition-SiC-precoated C/C–SiC: thermodynamic assessment and high-temperature investigation. *J. Am. Ceram. Soc.*, 2005, **88**, 424–430.
21. Sun, Z. Q., Zhou, Y. C. and Li, M. S., Effect of $LiYO_2$ on the synthesis and pressureless sintering of Y_2SiO_5. *J. Mater. Res.*, 2008, **23**, 732–736.
22. Wang, J. Y., Zhou, Y. C. and Lin, Z. J., First-principle elastic stiffness of $LaPO_4$ monazite. *Appl. Phys. Lett.*, 2005, **87** (No. 051902).
23. Ching, W. Y., Electronic structure and bonding of all crystalline phase in the silica–yttria–silicon nitride phase diagram. *J. Am. Ceram. Soc.*, 2004, **87**, 1996–2013.
24. Saruhan, B., *Oxide-based Fiber-Reinforced Ceramic-Matrix Composites, Principles and Materials*. Kluwer Academic Publishers, Boston, 2003.
25. Sun, Z. Q., Zhou, Y. C., Wang, J. Y. and Li, M. S., γ-$Y_2Si_2O_7$, a machinable silicate ceramics: mechanical properties and machinability. *J. Am. Ceram. Soc.*, 2007, **90**, 2535–2541.
26. Wang, R., Pan, W., Jian, C., Fang, M., Cao, Z. and Luo, Y., Synthesis and sintering of $LaPO_4$ powder and its application. *Mater. Chem. Phys.*, 2003, **79**, 30–36.
27. Morgan, P. E. D. and Marshall, D. B., Ceramics composites of monazite and alumna. *J Am. Ceram. Soc.*, 1995, **78**, 1553–1563.

28. Marshall, D. B., Lawn, B. R. and Evens, A. G., Elastic/plastic indentation damage in ceramics: the lateral crake system. *J. Am. Ceram. Soc.*, 1982, **65**, 561–566.
29. Cook, R. F., Lawn, B. R. and Fairbanks, C. G., Microstructure-strength properties in ceramics. I. Effect of crack size on toughness. *J. Am. Ceram. Soc.*, 1985, **68**, 604–615.
30. Hay, R. S. and Marshall, D. B., Deformation twining in monazite. *Acta Mater.*, 2003, **51**, 5235–5254.
31. Choudhry, M. A. and Islam, M., Twinning modes of $Er_2Si_2O_7$. *J. Mater. Sci.*, 2005, **40**, 3745–3747.
32. Choudhry, M. A., Javed, M. Z. and Bano, B., Twinning modes of $Nb_2Si_2O_7$. *Mater. Chem. Phys.*, 2007, **10**, 251–254.